VII. NOISE IN ELECTRON DEVICES

Prof. H. A. Haus
Prof. R. P. Rafuse
H. J. E. H. Pauwels
Prof. P. L. Penfield, Jr.
V. K. Prabhu

RESEARCH OBJECTIVES

Our present and future efforts are concentrated in three areas. The first concerns the noise performance of devices in which quantum effects are detectable or, in fact, dominant. Because it is relatively convenient to make amplitude noise measurements on the cw gaseous maser oscillator, the theoretical and experimental work is being done on this device.

(a) A quantum-mechanical analysis of the noise in optical maser oscillators is in progress. The purpose of the analysis is to determine the limitations of the semiclassical analysis.

(b) Measurements on the amplitude noise in optical maser oscillators will continue. Our intent is to use the noise measurements on "quiet" optical maser oscillators, as described in this report, to determine experimentally physical parameters of the gaseous discharge.

The second area of interest is noise in frequency multipliers, especially in those made from varactors. We hope to develop simple parameters to indicate the noisiness of a signal and of a multiplier through which this signal passes, and then to compare the noise performance of various types of multiplier chains.

The third area of interest is the noise contribution of double-sideband degenerate parametric amplifiers in a variety of applications.

H. A. Haus, P. L. Penfield, Jr., R. P. Rafuse

A. MEASUREMENT OF AMPLITUDE NOISE IN OPTICAL CAVITY MASERS

Measurements on the amplitude noise of a cavity-type gaseous optical maser oscillator operating at 6328 Å above and below threshold are reported here. The measurements show that the noise is due mainly to spontaneous emission.

The measurements above threshold are similar to those reported by Prescott and Van der Ziel[1]; however, we report more data taken above threshold so that several theoretical predictions may be checked. Furthermore, we compare these measurements with measurements taken below threshold, and thus are able to confirm the fact that the source of noise below and above threshold is the same. Finally, we compare our results above threshold with the theory of noise in Van der Pol oscillators,[2] not with the linear theory as Prescott and Van der Ziel[1] did. The former theory is the proper one to use for the maser oscillator,[3] and is found to be in good quantitative agreement with experiments. We use the theory previously discussed[2] as applied to the equivalent circuit of Fig. VII-1. The conductance $G = \omega_o C/Q$ represents the loading of the resonator by the outside space. $G_m = G_m^o(1-aV^2) = \omega_o C/Q_m$ is the (usually negative) conductance of the maser material. Above threshold, the

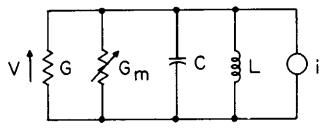

Fig. VII-1. Equivalent circuit of the noisy oscillator.

magnitude of the negative conductance G_m decreases quadratically with voltage. The uniform spectral density $\overline{i^2}/\Delta\nu = 4G_m h\nu\Delta\nu(n_2/g_2)/(n_1/g_1 - n_2/g_2)$ of the noise current generator is chosen so that the power emitted by the cavity below threshold corresponds to a well-known linear result.[4] Here, n_1 and n_2 are the populations of the lower and upper levels, respectively, and g_1 and g_2 are their degeneracies. It is assumed that above threshold the dependence of the noise power upon the population inversion is the same as that below threshold. When the noise power obtained from the equivalent circuit is incident on a photomultiplier, the photoemission theory of Mandel[5] gives for the spectrum $S(\nu)$ of the photomultiplier current, with the maser operating above, but near, threshold

$$S(\nu) = 2Ae\Gamma I_a + 4AeI_a\eta \frac{n_2/g_2}{n_2/g_2 - n_1/g_1}\left(\frac{\Delta\nu_o}{\Delta\nu}\right)^2 \frac{1}{1+\left(\frac{\nu}{\Delta\nu}\right)^2} \equiv S_s + S_e. \tag{1}$$

Here, e is the electron charge; A, the photomultiplier gain; Γ, the shot-noise enhancement factor resulting from secondary emission; η, is a loss factor including the quantum efficiency and all losses between the maser output and photomultiplier, and

$$\Delta\nu = \nu_o\left(\left|\frac{1}{Q_m^o}\right| - \frac{1}{Q}\right), \tag{2}$$

where ν_o is the frequency of the laser oscillation, $\Delta\nu_o = \nu_o/Q$ is the half-power bandwidth of the cavity.

This expression differs in two respects from equation (5) of Prescott and Van der Ziel[1] when the latter is applied to near-threshold operation. The amplitude of the second term in (1) is smaller by a factor of 8, and the bandwidth (2) is larger by a factor of 2.

Below, but near, threshold, for $S(\nu)$ one finds the same expression (1) except that $\Delta\nu$ is given by

$$\Delta\nu = \nu_o\left(\frac{1}{Q} + \frac{1}{Q_m^o}\right) \qquad Q_m^o \lesssim 0. \tag{3}$$

One should note, however, that below threshold contributions of other modes than the most strongly excited axial, linearly polarized mode become more and more important as the excitation is decreased.

In our experiments, an internal mirror laser of nearly hemispherical geometry, with a mirror spacing of 50 cm, was used. The I. D. of the quartz tube was approximately 3.5 mm. The gas pressure was ~1.5 mm Hg, with a 10:1 ratio of the partial pressures of He and Ne. The maser was DC-excited; gas-discharge fluctuations were suppressed

by a magnet near the discharge. The maser was stabilized to less than 1 per cent long-term drift in amplitude by means of a feedback circuit with a time constant of 1/50 sec by using the light emerging from one of the maser mirrors. The light through the other mirror was fed partly to a photomultiplier connected to a counter, and partly to a photomultiplier used in conjunction with spectrum analyzers. The spectrum was studied in the range 0-17 Mc. Different spectrum analyzers were used for the various ranges of the frequency spectrum. The scanning velocities ranged from 1-4 cps/sec at the low-frequency end to 250-1000 cps/sec near the high-frequency position of the spectrum. The corresponding IF bandwidths ranged from a minimum of 10 cps to a maximum of 10,000 cps. The spectrum analyzer output was fed into a spectral density analyzer with integration times in the range 1-5 sec, and then to a chart recorder.

The composite experimental results are shown in Fig. VII-2. The curves are labeled by the photoelectron count $\bar{N}$ at the photomultiplier cathode. Above threshold (Fig. VII-2a), six dynodes of the photomultiplier were shorted out. The curves below threshold clearly show the narrowing of the bandwidth and the rise of the excess noise level S_e over the shot noise S_s as the threshold is approached from below. Lorentzian curves can be fitted with very good accuracy onto the top curves.

The curves obtained with the maser operating above threshold show a decrease of S_e/S_s with a simultaneous increase of the bandwidth as the maser power is increased. All experimental points can be fitted to Lorentzian curves. The two curves with the highest ratios S_e/S_s and the narrowest bandwidths represented the highest power below threshold and the lowest power above threshold at which our maser could operate stably and reproducibly for several months. The small spike modulation at approximately 170 kc above threshold is due to residual gas plasma oscillations.

The experimentally observed spectral curves of the photomultiplier current are predicted quantitatively by Eqs. 1-3.

1. The "saturation level" of the excess noise (near zero frequency), S_e, divided by the shot-noise level, S_s, is proportional to the maser power P below threshold and inversely proportional to P above threshold. A deviation occurs only farther below threshold when more than one single linearly polarized mode contributes to the output.

2. The bandwidth of the excess noise is inversely proportional to P below threshold and directly proportional to P above threshold.

3. The measured ratio S_e/S_s, above threshold by Eq. 1, gives for $n_2/g_2/(n_2g_2-n_1g_1)$ the reasonable value of 1.97, with the experimentally determined values of $\eta = 4.9 \times 10^{-3}$, $\Gamma = 1.3$, and $\Delta\nu_o = 4.7 \times 10^5$ cps as computed from the reflectance of the mirrors. Note that near threshold, both above and below it, with $Q \simeq Q_m^o$, the value of $(n_2/g_2)/(n_2/g_2-n_1/g_1)$ in (1) may be considered constant as compared with the rapid variation of $\Delta\nu_o/\Delta\nu$.

4. For equal bandwidths, the ratio of excess to shot noise above threshold is equal

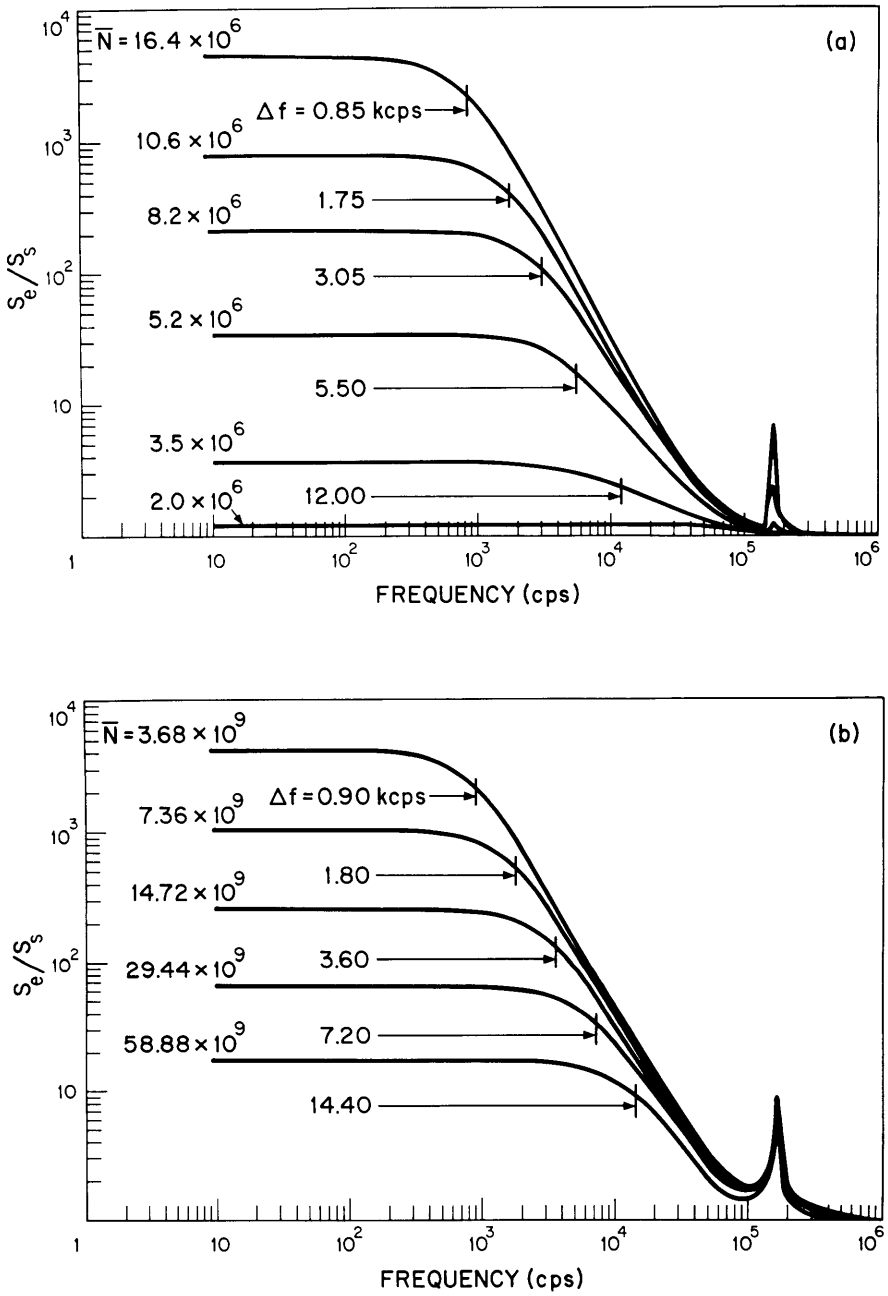

Fig. VII-2. Experimentally observed spectrum of photomultiplier current, normalized to shot noise: (a) above threshold; (b) below threshold.

to that below threshold, provided that one mode, with linear polarization, dominates both above and below threshold. Here we find that the predicted value of the ratio S_e/S_s from the result above threshold for the narrowest curve of the operation below threshold is 4600. The measured value is 4400.

The measurements were carried out at Lincoln Laboratory, M. I. T., in cooperation with Mr. Charles Freed.

H. A. Haus

References

1. L. J. Prescott and A. Van der Ziel, Detection of spontaneous emission noise in He-Ne lasers, Phys. Letters 12, October 15, 1964.

2. H. A. Haus, Quarterly Progress Report No. 72, Research Laboratory of Electronics, M. I. T., January 15, 1964, pp. 53-56.

3. W. E. Lamb, Theory of an optical maser, Phys. Rev. 134, 6A (1964).

4. M. W. Mueller, Noise in molecular amplifier, Phys. Rev. 106, 8-13 (1957).

5. L. Mandel, Fluctuations of photon beams: The distribution of the photoelectrons, Proc. Phys. Soc. (London) 74, Pt. 3, 233-43 (September 1959); see also Quarterly Progress Report No. 71, Research Laboratory of Electronics, M. I. T., October 15, 1963, pp. 87-90.

B. NOISE PERFORMANCE OF ABRUPT-JUNCTION VARACTOR FREQUENCY DOUBLER

1. Characterization of Noise in Varactor Frequency Multipliers

A sinusoidal signal corrupted by narrow-band noise can be represented as

$$f(t) = 2\ \mathrm{Re}\left\{V_s + x(t) + jy(t)\right\} e^{j\omega_o t}. \tag{1}$$

It can be proved that an equally good representation for f(t) is

$$f(t) = 2\ \mathrm{Re}\left[V_s + V_\alpha e^{j\omega t} + V_\beta^* e^{-j\omega t}\right] e^{j\omega_o t}. \tag{2}$$

In most of the cases of practical interest the signal power is very much larger than the noise power; and we have assumed in our analysis that

$$\overline{|V_\alpha + V_\beta|^2} \ll V_s^2 \tag{3}$$

$$\overline{|V_\alpha - V_\beta|^2} \ll V_s^2. \tag{4}$$

A typical power spectrum of f(t) is shown in Fig. VII-3.

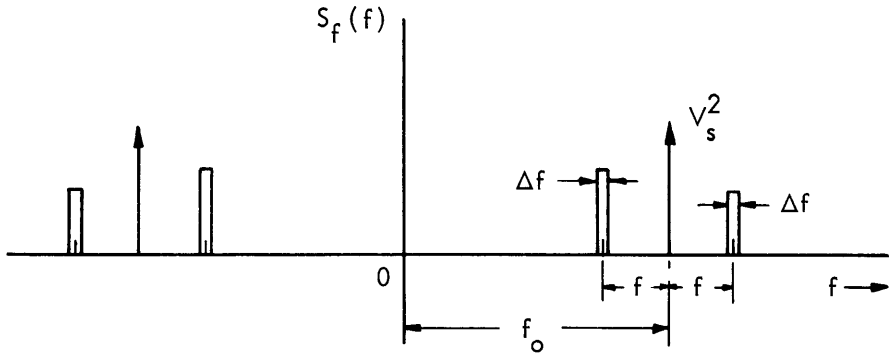

Fig. VII-3. Power spectrum of f(t).

2. Definition of Amplitude Noise, Phase Noise, and a Set of Figures of Merit

In the present analysis, we shall deal exclusively with the spot-noise performance[2] of multipliers.

The signal f(t) in (1) (under our assumption of high signal-to-noise ratio) may be written[4]

$$f(t) \doteq 2\{V_s+x(t)\} \cos\left[\omega_o t + \frac{y(t)}{V_s}\right]. \tag{5}$$

We shall, therefore, refer to x(t) as the amplitude noise, and to y(t) as the phase noise.

The instantaneous amplitude of f(t) is given by

$$R(t) \doteq 2\{V_s+x(t)\}, \tag{6}$$

and the instantaneous angular frequency of f(t) is

$$\omega_i(t) \doteq \omega_o + \frac{y'(t)}{V_s}. \tag{7}$$

The amplitude noise figure F_2 is defined as

$$F_2 = (S/N_{AM})_{in} \Big/ (S/N_{AM})_{out}, \tag{8}$$

where $(S/N_{AM})_{in}$ is the exchangeable signal-to-amplitude noise ratio of the input network; and $(S/N_{AM})_{out}$ is the signal-to-amplitude noise ratio across the load.

The phase noise figure F_3 is defined as

$$F_3 = (S/N_{PH})_{in} \Big/ (S/N_{PH})_{out}, \tag{9}$$

where $(S/N_{PH})_{in}$ and $(S/N_{PH})_{out}$ are the exchangeable signal-to-phase noise ratio of the

input network and the signal-to-phase ratio across the load, respectively.

3. Noise Performance of Lossless Varactor Frequency Multipliers

A functional representation of a varactor multiplier is given in Fig. VII-4. R_{in}, as shown in Fig. VII-4, is the input resistance of the varactor multiplier.

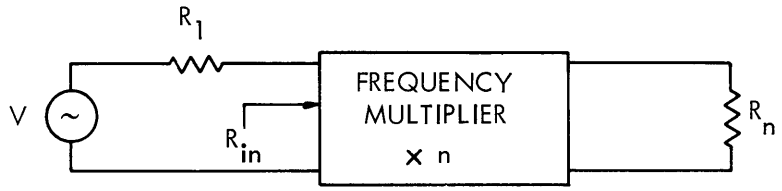

Fig. VII-4. Varactor frequency multiplier.

With the noise sources in the bias network neglected, and the bias source admittance zero, we have shown that, for a doubler,

$$F_3 = 4 \tag{10}$$

$$F_2 = 4/(3-2\lambda_o)^2, \tag{11}$$

where

$$\lambda_o = R_{in}/(R_{in}+R_1). \tag{12}$$

It is interesting to see that $F_2 = 1$ for $\lambda_o = 1/2$, or $R_{in} = R_1$. This has also been shown to be true for higher order mutlipliers. The value of F_3 for an n^{th}-order multiplier has been proved to be n^2.

4. Noise Performance of an Abrupt-Junction Doubler

Let m_1 and m_2 be the modulation ratios of the doubler; and let T_d be the noise temperature of the parasitic series resistance, R_s, of the varactor.

With the noise statistics of the input termination given by

$$\overline{|V_\alpha+V_\beta|^2} = 4kT_A R_1 \Delta f \tag{13}$$

$$\overline{|V_\alpha-V_\beta|^2} = 4kT_P R_1 \Delta f \tag{14}$$

and

$$\overline{[V_\alpha-V_\beta][V_\alpha+V_\beta]^*} = \rho\sqrt{\overline{|V_\alpha-V_\beta|^2}}\sqrt{\overline{|V_\alpha+V_\beta|^2}}, \tag{15}$$

we have shown that

$$F_2 - 1 = \frac{3 + 4m_2 \frac{\omega_c}{\omega_o} + 4 \frac{T_d}{T_A}\left(1 + m_2 \frac{\omega_c}{\omega_o}\right)\left\{1 + \frac{4m_2^2}{m_1^2}\left(1 + \frac{1}{m_2}\frac{\omega_o}{\omega_c}\right)^2\right\}}{\left(1 + 2m_2 \frac{\omega_c}{\omega_o}\right)^2}. \tag{16}$$

In this analysis we have assumed that the average elastance, S_o, of the varactor has been tuned out; and the formula (16) has been derived for the case $R_{in} = R_1$.

For the doubler with optimum efficiency, the asymptotic low-frequency value of F_2 is

$$F_2 - 1 = \left(12.50 + 19.87 \frac{T_d}{T_A}\right)\frac{\omega_o}{\omega_c}. \tag{17}$$

The asymptotic high-frequency value of F_2 under the same conditions is given by

$$F_2 - 1 = 3 - 0.0624\left(\frac{\omega_c}{\omega_o}\right)^2 + \frac{T_d}{T_A}\left[2.4976 + 64\left(\frac{\omega_o}{\omega_c}\right)^2\right]. \tag{18}$$

If the noise source in the bias network is indicated by V_o, and the impedance of the bias source is R_o, it has been shown that for the doubler with optimum efficiency, F_3 has the asymptotic low-frequency value

$$\begin{aligned} F_3 - 4 = {} & \frac{1.967}{4\left(1 + \frac{R_o}{R_s}\right)^2\left(\frac{\omega}{\omega_c}\right)^2 + 1}\frac{T_A}{T_P} + \frac{T_d}{T_P}\left(50 + \frac{50.4}{4\left(1 + \frac{R_o}{R_s}\right)^2\left(\frac{\omega}{\omega_c}\right)^2 + 1}\right)\frac{\omega_o}{\omega_c} \\ & - \frac{11.20}{4\left(1 + \frac{R_o}{R_s}\right)^2\left(\frac{\omega}{\omega_c}\right)^2 + 1}\frac{\omega_o}{\omega_c}\left[\left(1 + \frac{R_o}{R_s}\right)\left(\frac{\omega}{\omega_o}\right)\mathrm{Re}\,\rho + \frac{1}{2}\frac{\omega_c}{\omega_o}\mathrm{Im}\,\rho\right]\sqrt{\frac{T_A}{T_P}} \\ & + \frac{34.6}{4\left(1 + \frac{R_o}{R_s}\right)^2\left(\frac{\omega}{\omega_c}\right)^2 + 1}\frac{\omega_o}{\omega_c}\frac{\overline{V_o^2}}{4kT_P R_s \Delta f}. \end{aligned} \tag{19}$$

The analysis shows, therefore, that the minimum possible values of amplitude and phase noise figures for an abrupt-junction varactor frequency doubler are 1 and 4, respectively.

Similar formulas have been developed for higher order multipliers, and the methods

of optimization of these figures of merit are now under investigation.

V. K. Prabhu

References

1. W. B. Davenport, Jr. and W. L. Root, An Introduction to the Theory of Random Signals and Noise (McGraw-Hill Book Company, Inc., New York, 1958).

2. H. A. Haus and R. B. Adler, Circuit Theory of Linear Noisy Networks (The Technology Press of M. I. T., Cambridge, Mass. and John Wiley and Sons, Inc., New York, 1959).

3. P. Penfield, Jr. and R. P. Rafuse, Varactor Applications (The M. I. T. Press, Cambridge, Mass., 1962).

4. S. O. Rice, Mathematical analysis of random noise, Bell System Tech. J. 23, 282-332 (1944); 24, 46-156 (1945).